ACS Photonics

pubs.acs.org/journal/apchd5

Article

Rapid Infrared Spectroscopic Nanoimaging with nano-FTIR Holography

Martin Schnell,* Monika Goikoetxea, Iban Amenabar, P. Scott Carney, and Rainer Hillenbrand

Cite This: *ACS Photonics* 2020, 7, 2878–2885

Read Online

ACCESS | Metrics & More | Article Recommendations | Supporting Information

ABSTRACT: Scattering-type scanning near-field optical microscopy (s-SNOM) and its derivate, Fourier transform infrared nanospectroscopy (nano-FTIR), are emerging techniques for infrared (IR) nanoimaging and spectroscopy, with applications in diverse fields ranging from nanophotonics, chemical imaging, and materials science. However, spectroscopic nanoimaging is still challenged by the limited acquisition rate of current nano-FTIR technology. Here we combine s-SNOM, nano-FTIR, and synthetic optical holography (SOH) to achieve infrared spectroscopic nanoimaging at unprecedented speed (eight spectroscopically resolved images in 20 min), which we demonstrate with a polymer composite sample. Beyond being fast, our method promises to enable nanoimaging in the far IR spectral range, which is covered by IR supercontinuum and synchrotron sources, but not by current quantum cascade laser technology.

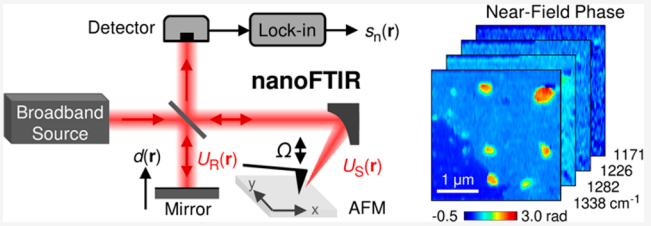

KEYWORDS: *scattering-type scanning near-field optical microscopy (s-SNOM), synthetic optical holography, infrared nanoimaging, infrared nanospectroscopy, interferogram bandpass sampling*

Scattering-type scanning near-field optical microscopy (s-SNOM)[1] is an emerging tool for infrared (IR) nanoimaging that extends the analytical power of infrared light to the deep subwavelength scale. It has thus found successful application in a variety of fields, including the nanoscale identification of molecular vibration signatures,[2−6] the probing of polaritonic excitations in novel nanophotonic structures,[7−10] the mapping of the free carrier concentration in semiconductors,[11−13] and the study of metal−insulator transitions and strongly correlated quantum materials.[14−17] In s-SNOM, the metal-coated tip of an atomic force microscope (AFM) is illuminated with monochromatic IR light and produces a tightly confined and strongly enhanced IR hot spot at the tip apex. When brought in proximity to a sample surface, the tip interacts with the sample via near-field coupling. Recording the tip-scattered light while the sample is being scanned yields a map of the local dielectric properties of the sample with nanoscale spatial resolution that is independent of the IR wavelength.[18,19] Interferometric recording of tip scattered light yields amplitude and phase images, revealing local refractive and absorptive properties.[20] Because the tip-scattered near field is a relatively weak signal, s-SNOM relies on high brilliance IR sources to efficiently focus IR light onto the AFM tip and to obtain sufficiently high signal-to-noise ratio (SNR). Development and refinement of IR light sources expanded the s-SNOM spectral range to cover molecular vibrations in the fingerprint region and many mid-IR polaritonic excitations and has thus provided the main driver in expanding the application potential of s-SNOM in the past decade. Current quantum cascade laser (QCL) technology[5,21] offers tunable, monochromatic IR emission between 1700 and 800 cm^{-1} at high output power and allows for routine IR nanoimaging to map heterogeneous structure, sample composition, or polaritonic excitation with high SNR.

The implementation of infrared broadband sources in s-SNOM enabled Fourier transform infrared nanospectroscopy (nano-FTIR), a derivate of s-SNOM that overcomes the diffraction-limited spatial resolution of conventional FTIR spectroscopy. In nano-FTIR, the AFM tip is illuminated with IR broadband radiation from thermal sources,[22−26] difference frequency generation (DFG),[4,27−30] or synchrotrons covering the entire mid-infrared range.[31−34] The tip-scattered light is analyzed with an asymmetric Fourier transform spectrometer, yielding IR amplitude and phase spectra with the spatial resolution of s-SNOM. Particularly for soft matter such as polymers and proteins, nano-FTIR phase spectra match well with standard infrared absorption spectra.[4,35] Nano-FTIR can thus provide unambiguous material identification based on the position and ratio of molecular and phonon resonances,[4−6,24,27−40] or verification of the nature of optical excitations by resolving the dispersion relation and propagation losses of polaritons.[9,41−43]

Received: July 23, 2020
Published: September 21, 2020

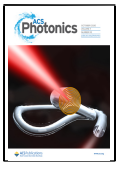

https://dx.doi.org/10.1021/acsphotonics.0c01164
ACS Photonics 2020, 7, 2878−2885

The combination of s-SNOM (mapping sample heterogeneity) with nano-FTIR (material identification) offers the most comprehensive sample characterization, which is particularly beneficial in the case of unknown samples. However, this poses a practical problem as both monochromatic and broadband infrared light sources need to be owned, which are expensive. Further, the spectral coverage of current QCL technology is limited in comparison to broadband infrared sources, and thus, QCL-based nanoimaging becomes impractical for frequencies below 800 cm^{-1} where many interesting material excitations abound.[44,45] It is thus desirable to develop a modality for spectroscopic infrared nanoimaging based on nano-FTIR. However, even with infrared supercontinuum lasers,[4] which offer the highest spectral irradiance among IR broadband sources, simple sequential acquisition of spectra is still a slow imaging method, typically requiring second-long acquisition times per spectrum and multiple hours per hyperspectral data set.[6] As the spectral irradiance of IR broadband laser technology continues to improve, it is the scanning mechanism of nano-FTIR that is increasingly becoming a bottleneck for imaging speed, that is, the piezo stage of the Michelson interferometer that needs to be scanned repeatedly for each spatial location to acquire an interferogram.

Recently, methods for nano-FTIR imaging at significantly reduced time scales were presented. Johnson et al. demonstrated spectroscopic nanoimaging of organic mineral interfaces, where the approach of a rotating frame from nuclear magnetic resonance (NMR) was adopted to sample vibration resonances at a reduced number of interferogram points.[46] Alternatively, compressive sensing has been implemented for spectroscopic nanoimaging of phonon resonances with synchrotron radiation, where the assumption of sparsity in the spectral domain was utilized to recover the nano-FTIR signal from a subsampled data set.[47] These first studies are encouraging and point to the potential of advanced spectral encoding algorithms for speeding up spectroscopic nanoimaging. Yet, reported acquisition times (few hours) have not yet reached those of monochromatic s-SNOM imaging with QCLs (few minutes). The practicality of spectroscopic nanoimaging will critically depend on performance metrics such as acquisition times, SNR and the degree of sample and interferometer drift, the limits of which remain to be explored for nano-FTIR.

Here, we have developed nano-FTIR holography based on synthetic optical holography (SOH) for rapid spectroscopic nanoimaging. To this end, we combine (i) interferogram bandpass sampling to significantly reduce the number of measurements and (ii) interferogram recording in form of a single synthetic hologram, from which the full spectroscopic data set can be reconstructed. We demonstrate nano-FTIR holography by spectroscopic nanoimaging of molecular resonances in a polymer test sample, yielding maps of 3800 spatial locations at eight frequency points within an effective imaging time of 20 min. We evaluate the SNR and obtain a precision in phase measurement in the range of 20 to 200 mrad (~1−10°), which is sufficient to resolve typical phonon resonances and moderately strong molecular resonances.

Basics of Synthetic Optical Holography. Synthetic optical holography (SOH)[48] is a recently introduced holographic modality of quantitative phase imaging in s-SNOM,[48,49] confocal microscopy,[50,51] and scanning cavity microscopy.[52,53] SOH was originally developed for s-SNOM imaging at a single laser line (single-frequency SOH) and forms the foundation for nano-FTIR holography. Briefly, in single-frequency SOH, the AFM tip is illuminated with light from a gas laser or QCL (Figure 1a). The tip-scattered field,

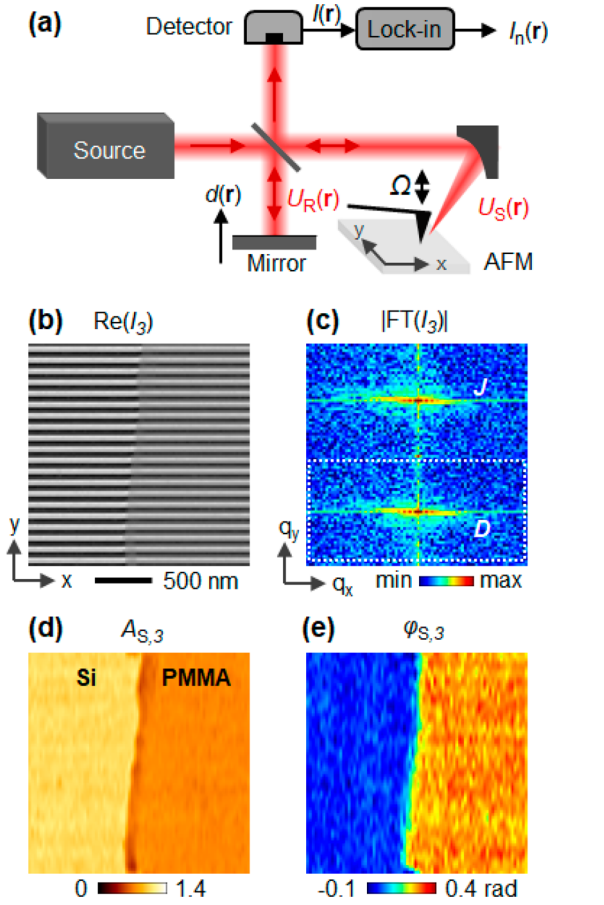

Figure 1. Infrared nanoimaging with synthetic optical holography and s-SNOM. (a) Setup. (b−e) Single-frequency SOH s-SNOM imaging of a spin-coated poly(methyl methacrylate) (PMMA) film on silicon substrate. (b) Near-field hologram recorded at 1731 cm^{-1}. (c) Fourier transform (FT) of the hologram, revealing direct (D) and conjugate (J) terms. (d, e) Reconstructed near-field amplitude and phase images, $A_{S,3}$ and $\varphi_{S,3}$. AFM: atomic force microscope; Lock-in: lock-in amplifier; Sample position $\mathbf{r} = (x,y)$; Reference mirror position along the optical axis $d(\mathbf{r})$; Tip-scattered field $U_S(\mathbf{r})$; Reference field $U_R(\mathbf{r})$; Demodulated detector signal $I_3(\mathbf{r})$.

$U_S(\mathbf{r}) = A_S(\mathbf{r})e^{i\varphi_S(\mathbf{r})}$, is collected with a parabolic mirror and superposed at the detector with a reference field, $U_R(\mathbf{r}) = A_S e^{i\varphi_R(\mathbf{r})}$. While the sample is rapidly scanned in position $\mathbf{r} = (x,y)$, the reference mirror of the interferometer is slowly translated to modulate the phase of the reference field, $\varphi_R(\mathbf{r}) = 2\pi \cdot 2d(\mathbf{r})/\lambda$, where λ is the wavelength of the laser line. Specifically, linear-in-time movement of the reference mirror generates a plane reference wave across the image, $U_R(\mathbf{r}) = A_R e^{i\mathbf{k}_\parallel \mathbf{r}}$, with in-plane wave vector, $\mathbf{k}_\parallel$. To suppress background contributions, the AFM tip is vertically vibrated at frequency Ω, and the detector signal, $I(\mathbf{r})$, is demodulated with a lock-in amplifier at the nth order of the tip vibration frequency, $n\Omega$, yielding the demodulated detector signal, $I_n(\mathbf{r})$. By recording $I_n(\mathbf{r})$ pixel-by-pixel, a synthetic near-field hologram is obtained (Figure 1b), which exhibits a regular fringe pattern that is reminiscent of classical off-axis holography. Performing two-

https://dx.doi.org/10.1021/acsphotonics.0c01164
ACS Photonics 2020, 7, 2878−2885

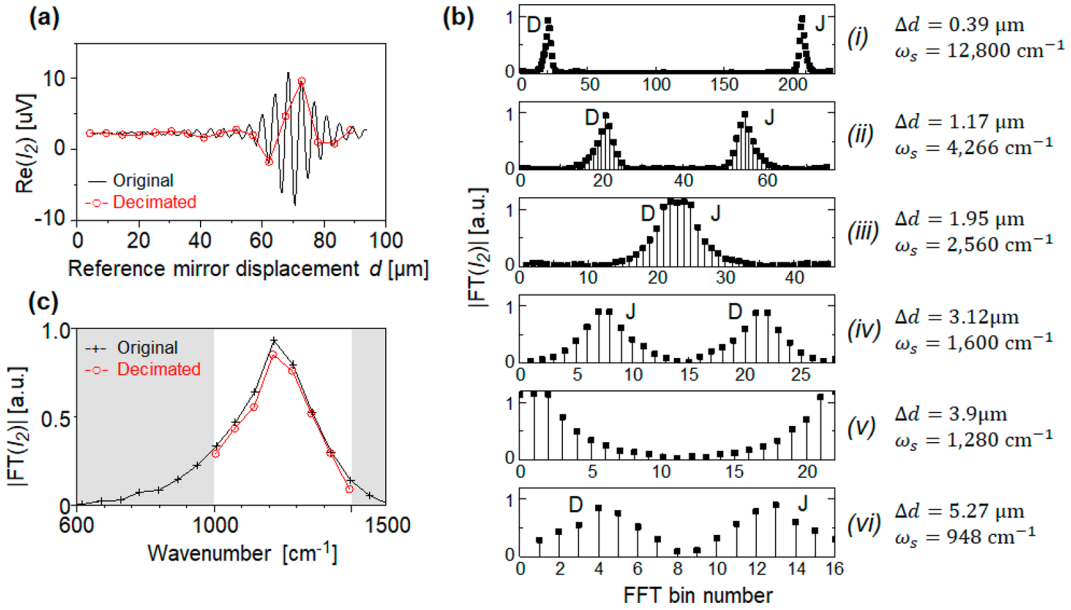

Figure 2. Bandpass sampling as a strategy to significantly reduce the number of interferogram points at the same spectral resolution in nano-FTIR. (a) Nano-FTIR interferogram on Si. (b) Fourier transform (FT) of the interferogram in (a) when resampled at different rates: (i) original sampling interval Δd = 0.39 μm, (ii–vi) subsampled data sets. Labels "D" and "J" mark direct and conjugate spectra, respectively. (c) FT of the original (black, Δd = 0.39 μm) and decimated (red, Δd = 5.27 μm) interferograms in (a), validating spectral fidelity for interferogram bandpass sampling. Acquisition parameters: 90 μm total interferogam length, 230 pixel, 10 ms integration time, and 32-fold spectral averaging.

dimensional Fourier transform (FT) of the hologram yields a direct term (labeled "D") and a conjugate term ("J") that have separated into the lower and upper halfspaces of the FT plane, respectively (Figure 1c). The direct term, $A_R^* \tilde{U}_{S,n}$, and its conjugate, $A_R \tilde{U}_{S,n}^*$, are the FT of the n-th coefficient of the time-harmonic coefficient of the tip-scattered field, $U_{S,n}(\mathbf{r}) = A_{S,n}(\mathbf{r}) e^{i\varphi_{S,n}(\mathbf{r})}$, shifted by $\mathbf{k}_\parallel$ and $\mathbf{k}_\parallel$, respectively (tilde indicates FT with respect to position). Reconstruction of the near-field amplitude and phase images, $A_{S,n}(\mathbf{r})$ and $\varphi_{S,n}(\mathbf{r})$, can be done straightforwardly by spatial filtering of the direct term in the FT of the hologram (indicated by the dashed rectangle in Figure 1c), recentering and performing an inverse FT (for details, see ref 48). The presented example (Figure 1c–e) is a spin-coated poly(methyl methacrylate) (PMMA) film, which exhibits well-defined molecular vibrational resonances, supported by a silicon substrate. With the laser tuned to the C=O stretching bond of PMMA, the near-field phase image reveals strong absorption in the PMMA film (Figure 1e, region of positive phase contrast).[54]

Interferogram Bandpass Sampling. We illustrate and demonstrate nano-FTIR holography by implementing it in a commercial near-field microscope (NeaSNOM, Neaspec GmbH, Munich) using its nano-FTIR module (Figure 1a, source is now a IR broadband source). We first show that the medium spectral bandwidth of OPO/DFG sources (a few 100s of cm^{-1}), as used in nano-FTIR, provides an opportunity for bandpass sampling[55] of the interferogram, that is, sampling the interferogram at a rate below Nyquist. Such bandpass sampling can be applied to significantly reduce the number of interferogram points and thus speed up data acquisition by more than a magnitude compared to conventional nano-FTIR. To this end, the DFG source of the nano-FTIR module was set to emit in the spectral range from 1000 to 1400 cm^{-1} (range "B") at 350 μW spectrally integrated power. As near-field probes, we employed metalized atomic force microscope (AFM) cantilevers (ARROW-NCPt, NanoWorld AG, Switzerland) that were vibrated vertically at 80 nm amplitude and 270 kHz frequency. The infrared detector signal was demodulated at the second harmonic of the tip vibration frequency to suppress background contributions.

Figure 2a shows a typical nano-FTIR interferogram recorded on silicon, a spectrally flat test sample. The Fourier transform (FT) of the interferogram revealed that signal content was limited to a narrow frequency band close to zero (DC) frequency (Figure 2b, plot (i)). This is because the interferogram was sampled at high rate as typical in nano-FTIR, that is at intervals of Δd = 0.39 μm, which translates to a sampling frequency $\omega_s = 1/(2\Delta d)$ = 12800 cm^{-1} (the factor of 2 takes into account the round trip of the reference beam) or at 4.5× the Nyquist rate with respect to the highest frequency (1400 cm^{-1}). This form of sampling is referred to as oversampling. As a strategy to reduce the number of interferogram points, we apply bandpass sampling from digital signal processing[55] to nano-FTIR. Subsampling the interferogram at no loss in information is possible in a range of sampling frequencies, ω_s, given by $\omega_s' \geq \omega_s \geq \omega_s''$, where the upper and lower frequency limits are given by

$$\omega_s' = 2\omega_{LO}/m \text{ and } \omega_s'' = 2\omega_{HI}/(m+1) \quad (1)$$

with m being the number of spectral replications (i.e., the degree of subsampling). Furthermore, the sampling frequency must be twice the source bandwidth, $\omega_s \geq 2BW = 2\omega_{HI} - \omega_{LO}$). For the given settings of the nano-FTIR source (ω_{HI} = 1400 cm^{-1} and ω_{LO} = 1000 cm^{-1}), valid ranges of sampling frequencies are thus 2000 cm$^{-1} \geq \omega_s \geq$ 1400 cm^{-1} (for m = 1) and 1000 cm$^{-1} \geq \omega_s \geq$ 933 cm^{-1} (for m = 2). Higher values $m \geq 3$ do not yield valid subsampling because the condition, $\omega_s \geq$ 2BW, is not fulfilled. To illustrate situations of valid and invalid subsampling, we simulated interferogram subsampling by resampling the original, oversampled interferogram (Figure 2a, black) at different intervals Δd and plotting the FT of the interferogram (Figure 2b). To ensure accurate simulations of

https://dx.doi.org/10.1021/acsphotonics.0c01164
ACS Photonics 2020, 7, 2878–2885

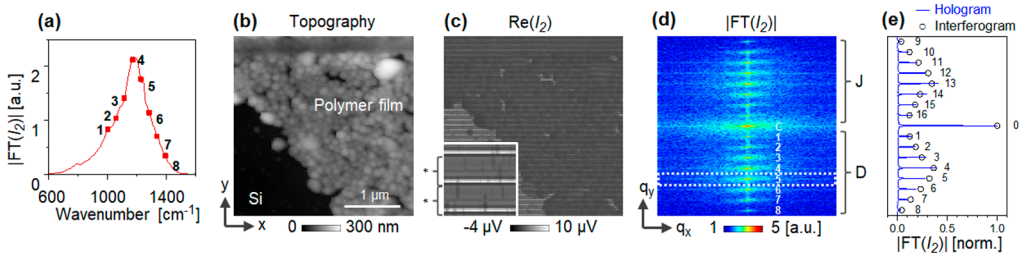

Figure 3. nano-FTIR holography enables rapid spectral imaging with nano-FTIR. (a) Bandwidth of the DFG source of the nano-FTIR module. (b) Topography of a polymer test film on silicon (Si). (c) Synthetic hologram acquired with the acquisition parameters as in Figure 2a, red points. Inset shows a digital zoom, revealing the hologram fringe pattern. The curly brackets (asterisk) next to the zoom mark the length of one bandpass sampled interferogram that is repeated in *y*-direction. (d) FT of the hologram, revealing term discretization and separation (plotted in logarithmic color scale). Labels "D" and "J" mark direct and conjugate terms, respectively. Direct terms are further labeled 1−8 in correspondence to the frequencies marked in (a). (e) Correspondence of the frequency bins of the bandpass-sampled interferogram in Figure 2b,vi (circles) with the terms in the FT of hologram (vertical line out across center of (d)). Note that hologram (c) and FT (d) (100 × 612 pixel) are displayed with an aspect ratio of 1:1 to reflect the real scan dimensions 3 μm × 3 μm.

bandpass sampling, integer multiples of the original sampling interval, Δd, were assumed and interpolation strategies were applied for noninteger multiples. The first two situations (plots (i) and (ii) in Figure 2b) correspond to oversampling ($\omega_s \geq 2\omega_{HI} = 2800$ cm^{-1}). The plots (iv) and (vi) represent cases of valid subsampling because direct and conjugate spectra clearly separate, while plots (iii) and (v) are cases of invalid subsampling because direct and conjugate spectra are overlapping (i.e., aliasing is present, which leads to data corruption). From plot (vi), Figure 2b, it is clear that interferogram sampling at $\Delta d = 5.27$ μm makes optimal use of the spectral bandwidth, while also providing separation between the near-field spectrum and its complex conjugate. Thus, correct reconstruction of the near-field spectrum is possible (red curve in Figure 2c), as it is verified by comparison with the spectrum of the original interferogram (black curve in Figure 2c). We note that bandpass sampling needs be configured to the specific frequency range of the nano-FTIR source, and thus, different sampling frequencies are needed for imaging in different spectral regions. By validating the bandpass sampling with a spectrally flat test sample, which directly reflects the source bandwidth, valid bandpass sampling is ensured for any sample.

Importantly, bandpass sampling resolves the near-field spectrum with the same number of frequency points (red circles) as oversampling (black circles) within the spectral range of the source (white area in Figure 2c). Thus, the reduction in interferogram points from 230 to 17 points promises a factor 13 faster imaging at no loss in spectral resolution. This reduction is valid under the assumption that the IR source is previously known to be of limited spectral bandwidth. We note that our source exhibited low and high frequency tails outside of the assumption of a bandlimited source (indicated by the gray areas in Figure 2c), that folded back on to the center of the spectrum and yielded slight distortion, which could explain the discrepancy in (Figure 2c, black vs red curve). These spectral tails of the source could be removed by optical filtering of the laser beam with infrared bandpass filters.

Nano-FTIR Holography. Direct implementation of bandpass sampling in conventional nano-FTIR spectroscopy is impractical because of the slow settling time of long travel piezo stages that move the reference mirror. To efficiently leverage the dramatic speed improvement afforded by interferogram bandpass sampling, we apply interferogram recording in form of synthetic holograms. To this end, we have adapted SOH to encode subsampled nano-FTIR interferograms across the image, a modality we designate as nano-FTIR holography. Specifically, at each position $\mathbf{r} = (x,y)$, the scattered field from the near-field probe, $U_S(\mathbf{r},\omega)$, is analyzed with an asymmetric Michelson interferometer where the tip is located in one arm of the interferometer (Figure 1a). Translation of the reference mirror, located in the other arm of the interferometer, samples the interferogram of the tip-scattered light. In contrast to conventional nano-FTIR, the position $d(\mathbf{r})$ of the reference mirror is held constant during the acquisition of a line scan (here assumed in the *x*-direction) and is moved to the next position after the completion of a line scan. Thus, while the AFM tip is rapidly scanned over the sample surface, the reference mirror is stepped through the positions specified in the decimated interferogram in Figure 2a (red points) for every line *y*, which effectively encodes nano-FTIR interferograms across the image. We note that spectral fidelity is robust to small global offsets in the reference mirror positions (see Supporting Information, note S1). The signal of the mercury cadmium telluride (MCT) detector, $I(\mathbf{r})$, is demodulated at the *n*th order of the tip vibration frequency, Ω, to suppress background contributions and thus extract the local near field scattered by the tip. By recording the demodulated signal, $I_n(\mathbf{r})$, pixel-by-pixel, we obtain a synthetic near-field hologram with nano-FTIR. Such holograms exhibit a regular, horizontal fringe pattern that is periodic in the *y* direction (Figure 3c, obtained with a polymer test sample, see below). The curly brackets in the zoom of Figure 3c indicate the period length, that is, the length of one interferogram. Importantly, the FT of the hologram shows clear term separation into numerous direct terms (labeled "D"), conjugate terms (labeled "J") and one autocorrelation term (labeled "C" in Figure 3d). The *m*th direct term corresponds to the *m*th frequency bin of the direct spectrum, as illustrated in Figure 3e. Thus, spectrally resolved near-field amplitude and phase images, $A^m_{S,n}(\mathbf{r})$ and $\varphi^m_{S,n}(\mathbf{r})$, can be straightforwardly reconstructed by (i) spatial filtering in the FT of the hologram, as exemplarily indicated by the dashed box in Figure 3d, (ii) recentering, and (iii) performing an inverse FT for each direct term. The resulting data set spectrally resolves the tip-scattered field, $U_S(\mathbf{r},\omega)$, at the same frequency points and with the same spectral resolution as with the bandpass-sampled interferogram (Figure 2c). We note that the original implementation of SOH, that is, linear-in-time movement of the reference mirror, will

https://dx.doi.org/10.1021/acsphotonics.0c01164
ACS Photonics 2020, 7, 2878−2885

not work in nano-FTIR because (i) the limited coherence length of broadband sources introduces diminishing fringe contrast toward the hologram periphery[56] and (ii) a continuous source spectrum would yield overlap of terms in the FT of the hologram, preventing spectroscopic resolution of near-field amplitude and phase images.

EXPERIMENTAL RESULTS

We tested our method by imaging a polyvinyledene fluoride and hexafluoropropylene copolymer (FP) film of 100 nm thickness on a silicon substrate that contained FP particle aggregates of ~100 to 400 nm size with a slightly shifted spectral response (film absorption peak near 1120 cm^{-1} versus aggregate absorption peak near 1160 cm^{-1}, see Methods for details). The sample topography is shown in Figure 3b. Hologram acquisition was performed by stepping the reference mirror in intervals of Δd = 5.27 μm for every completed line scan; thus, bandpass sampling the interferogram with the parameters previously established in Figure 2b, plot (vi), and with the same instrument settings. The resulting synthetic hologram exhibited a horizontal fringe pattern that repeated every 17 lines (Figure 3c). FT of the hologram reveals eight discrete direct terms in the lower half space (Figure 3d, labeled 1−8), which correspond to center frequencies between 1000 and 1400 cm^{-1}, as indicated in Figure 3a. Near-field amplitude and phase images (Figure 4a) were reconstructed from the FT of the hologram (Figure 3d), as described above, spatially and spectrally resolving the different sample constituents. We note that we applied 6× spatial oversampling in hologram recording in the slow scanning direction (y-axis) to partially compensate for the reduced spatial resolution in the reconstructed images, which yield an effective number of 100 × 38 pixels (see Supporting Information, note S2).

We next demonstrate the analytical capabilities of spectroscopic nanoimaging with broadband SOH (Figure 4a). Spatial features on the sample were recorded with 30 nm pixel size across an area of 3 μm × 3 μm and spectral features with 55 cm^{-1} resolution in the range of 1000 to 1400 cm^{-1}. This capability allowed for clear identification of the FP polymer film based on molecular absorption observed as a peak in the near-field phase of ~0.6 rad at 1226 cm^{-1}. The FP particle aggregates exhibited stronger response in phase (~2 rad) and amplitude (~1.2) peaking at 1170 and 1114 cm^{-1}, respectively. The measured absorption bands were reproduced by nano-FTIR spectroscopy in peak position, peak height, and peak shape, as revealed by direct comparison at selected locations on the sample (Figure 4b). This confirmed that nano-FTIR holography provided accurate near-field spectral data. Figure 4c quantifies noise levels in the near-field phase at regions of the FP film and the Si substrate, which are representative for typical low and high refractive index materials, respectively. We observed that the standard variation of the near-field phase generally scaled with the input power of the broadband source and the near-field amplitude response of the material. Thus, nanoimaging with phase sensitivity of ~20 mrad (~1°, on Si) and ~40 mrad (~2°, on FP polymer film) was possible near the center of the source emission. Lowest (1) and highest (8) frequency bins yielded higher phase noise and are thus not shown here. We provide further validation of nano-FTIR holography in a simulation in Supporting Information, note S3.

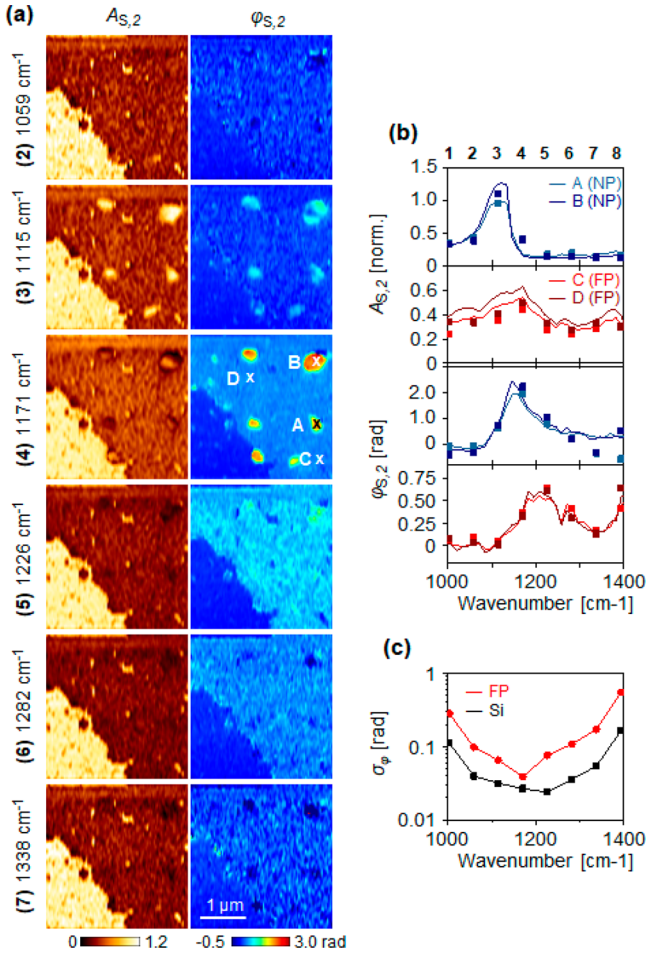

Figure 4. Demonstration of rapid spectroscopic imaging with a polymer test sample. (a) Spectral near-field amplitude and phase images, $A_{S,2}$ and $\varphi_{S,2}$, reconstructed from the hologram in Figure 3c and normalized to silicon. (b) Comparison of near-field phase as obtained from the spectral data set in (a) with nano-FTIR spectroscopy, both taken at locations A−D. (c) Standard deviation of the near-field phase as obtained from regions of FP (fluorine copolymer) and Si (silicon).

DISCUSSION

Nano-FTIR holography is based on interferogram bandpass sampling and thus offers opportunity to trade signal-to-noise ratio for high imaging speed, which cannot be easily done in conventional nano-FTIR imaging. In the presented experiment, we assumed a typical imaging scenario in s-SNOM where field of view (9 μm^2), spatial (30 nm in x and 80 nm in y directions) and spectral resolution (55 cm^{-1}) are sufficient to locate and identify many molecular and phonon resonances. While spectroscopic nanoimaging with conventional nano-FTIR spectroscopy can be expected to take hours, our experiments showed that such spectroscopic imaging can now be done on the time scale of 20 min. To our knowledge, this is the fastest demonstration of spectroscopic nanoimaging with a broadband source to date and it approaches the performance of near-field imaging with QCL.

In nano-FTIR holography, the spectral resolution is defined by the interferogram length L. Specifically, for a given source bandwidth, BW, and sampling rate, ω_s, the number of interferogram points, $N = (\omega_s/\Delta\omega)$, scales with spectral resolution, $\Delta\omega \sim 1/(2L)$ and the number of the resulting

https://dx.doi.org/10.1021/acsphotonics.0c01164
ACS Photonics 2020, 7, 2878−2885

spectral images is given by (BW/$\Delta\omega$). This implies that more interferogram points N need to be acquired when a better spectral resolution, $\Delta\omega$, is desired (longer interferograms), as it is also the case for nano-FTIR spectroscopy. However, bandpass sampling offers a further degree of freedom by allowing for trading source bandwidth, BW, for spectral resolution, $\Delta\omega$. In this case, longer interferograms can be sampled in larger steps, Δd, and at constant number of points, N, if the source bandwidth, BW, is reduced. Regular nano-FTIR spectroscopy does not benefit from such bandpass sampling because it is mechanically difficult to rapidly translate the reference mirror across long distances. Nano-FTIR holography, in contrast, can take full advantage of bandpass sampling because line scans are rapidly acquired for fixed reference mirror position, with a translation of the reference mirror only being required at the end of a line scan, which is mechanically easy to do. Thus, the speed advantage of nano-FTIR holography over regular nano-FTIR spectroscopy is particularly pronounced when spectral imaging at high spectral resolution and narrow source bandwidth. A possible application of our method could be the rapid imaging of small peak shifts (as in IR nanoimaging of structural protein heterogeneity[5]) by tailoring the source spectrum to the specific, narrow spectral region that encompasses the molecular absorption peaks of interest. The needed narrow-band sample illumination can be provided either directly using high-power IR sources with medium-sized spectral bandwidth[57] or by employing infrared bandpass filters, commercially available from several vendors, to reduce the source bandwidth of IR supercontinuum or synchrotron sources. In principle, our method can be extended to cover several disjoint regions in the IR spectral range, which would be useful for probing multiple absorption bands at very different frequencies simultaneously. To this end, the source spectrum could be tailored to cover just a narrow region around each absorption band (e.g., with optical bandpass filters) and bandpass sampling would need to be adjusted such that all individual regions spectrally separate in the FT of the subsampled interferogram, which can be tested with the procedure illustrated in Figure 2.

Further, nano-FTIR holography provides two practical advantages over previous methods for spectral nanoimaging. First, spectral imaging with nano-FTIR holography only requires the acquisition of a single hologram, which is technically simple and fast. Particularly, the overhead of conventional nano-FTIR imaging is avoided, i.e. the repeated recentering of the sample (to correct for sample drift) and remeasuring of reference spectra (to compensate for interferometer drift) during data acquisition.[6] Second, sample drift does not affect spectral fidelity as long as this drift is small across the length of one interferogram (here, 17 lines of the hologram), which is easy to achieve. In comparison, previous methods for rapid spectroscopic imaging (e.g., ref 46) sampled the interferogram on an image-by-image basis, where each near-field image was acquired for a fixed position of the reference mirror, which requires correction of sample drift.

CONCLUSIONS

We have presented nano-FTIR holography for rapid spectroscopic nanoimaging with nano-FTIR that is based on interferogram bandpass sampling combined with synthetic optical holography. In particular, we demonstrated spectroscopic nanoimaging of vibrational resonances on the order of tens of minutes rather than hours, which could find application in routine imaging of phonon and molecular resonances that yield a moderately large near-field phase response. nano-FTIR holography provides a practical alternative for QCL-based nanoimaging in cases where (i) only the nano-FTIR module is available or (ii) nanoimaging outside the spectral range of QCLs is desired. This capability may enable the direct observation of polaritons in atomically thin materials and semiconductors, which abound the long wave IR spectral region below 800 cm^{-1},[44] and other low-energy excitations in solids,[45] where coverage by current QCL technology is sparse. Our method makes use of existing hardware (DFG laser, nano-FTIR module) and can be implemented in software. Beyond nano-FTIR, our method could also be implemented in other scanning methods, including FTIR microspectrometry and spectroscopic LIDAR, where the combination of an interferometer and a one-pixel detector could provide the function of a classical spectrometer and an array detector.

METHODS

Sample Preparation. The test sample was prepared using a water-based polymer dispersion (latex) of polyvinyledene fluoride (PVDF) and hexafluoropropylene (HFP) copolymer (95/5% in weight) made by emulsion polymerization, kindly supplied by The Chemical Engineering group of the University of Basque Country-POLYMAT. The final particle size of the latex was around 129 nm measured by Dynamic Light Scattering (DLS, Malvern Nanosizer). The latex was diluted at 0.2% solids content and mixed under stirring. Then, the sample was cast onto silicon wafer through spin coating and dried overnight at room temperature. The film yielded two different conformations consisting of a polymer film formed by particles that have coalesced and individual aggregates formed by particles that have not coalesced, as a result of the specific drying conditions. Nano-FTIR spectroscopy measurements confirmed that both conformations yielded slightly different spectral signatures, which are detected and imaged in the experiments in the main text: molecular absorption near 1220 cm^{-1} for the film and near 1170 cm^{-1} for the aggregates.

ASSOCIATED CONTENT

Supporting Information

The Supporting Information is available free of charge at https://pubs.acs.org/doi/10.1021/acsphotonics.0c01164.

S1. Interferogram bandpass sampling is robust to small global shifts in the reference mirror position d. S2. Acquisition time and oversampling considerations for nano-FTIR holography. S3. Simulation of nano-FTIR holography (PDF)

S4. Matlab script for the reconstruction of nano-FTIR holograms (ZIP)

AUTHOR INFORMATION

Corresponding Author

Martin Schnell − *CIC nanoGUNE BRTA, 20018 Donostia-San Sebastian, Spain; IKERBASQUE, Basque Foundation for Science, 48013 Bilbao, Spain;* orcid.org/0000-0003-3514-3127; Email: schnelloptics@gmail.com

Authors

Monika Goikoetxea − *CIC nanoGUNE BRTA, 20018 Donostia-San Sebastian, Spain*

https://dx.doi.org/10.1021/acsphotonics.0c01164
ACS Photonics 2020, 7, 2878−2885

Iban Amenabar − *CIC nanoGUNE BRTA, 20018 Donostia-San Sebastian, Spain;* orcid.org/0000-0001-9921-2721
P. Scott Carney − *The Institute of Optics, University of Rochester, Rochester, New York 14620, United States*
Rainer Hillenbrand − *IKERBASQUE, Basque Foundation for Science, 48013 Bilbao, Spain; CIC nanoGUNE BRTA and Department of Electricity and Electronics, UPV/EHU, 20018 Donostia-San Sebastian, Spain;* orcid.org/0000-0002-1904-4551

Complete contact information is available at: https://pubs.acs.org/10.1021/acsphotonics.0c01164

Notes

The authors declare the following competing financial interest(s): R.H. is a cofounder of Neaspec GmbH, a company producing scattering-type scanning near-field optical microscope systems, such as the one used in this study. M.S., R.H., and P.S.C. are authors of U.S. patent 9,213,313. The other authors declare no competing interests.

■ ACKNOWLEDGMENTS

M.S. acknowledges support by the European Union's Horizon 2020 research and innovation programme under the Marie Sklodowska-Curie Grant Agreement No. 655888 (SYNTOH). The authors further acknowledge financial support from the Spanish Ministry of Science, Innovation and Universities (National Project RTI2018-094830-B-100 and the Project MDM-2016-0618 of the Marie de Maeztu Units of Excellence Program) and the Basque Government (Grant No. IT1164-19). The authors thank Stefan Mastel for providing the SOH data shown in Figure 1.

■ REFERENCES

(1) Keilmann, F.; Hillenbrand, R. Near-Field Nanoscopy by Elastic Light Scattering from a Tip. In *Nano-Optics and near-Field Optical Microscopy*; Zayats, A. V., Richards, D., Eds.; Artech House nanoscale science and engineering; Artech House: Boston; London, 2009.
(2) Brehm, M.; Taubner, T.; Hillenbrand, R.; Keilmann, F. Infrared Spectroscopic Mapping of Single Nanoparticles and Viruses at Nanoscale Resolution. *Nano Lett.* **2006**, *6* (7), 1307−1310.
(3) Berweger, S.; Nguyen, D. M.; Muller, E. A.; Bechtel, H. A.; Perkins, T. T.; Raschke, M. B. Nano-Chemical Infrared Imaging of Membrane Proteins in Lipid Bilayers. *J. Am. Chem. Soc.* **2013**, *135* (49), 18292−18295.
(4) Huth, F.; Govyadinov, A.; Amarie, S.; Nuansing, W.; Keilmann, F.; Hillenbrand, R. Nano-FTIR Absorption Spectroscopy of Molecular Fingerprints at 20 Nm Spatial Resolution. *Nano Lett.* **2012**, *12* (8), 3973−3978.
(5) Amenabar, I.; Poly, S.; Nuansing, W.; Hubrich, E. H.; Govyadinov, A. A.; Huth, F.; Krutokhvostov, R.; Zhang, L.; Knez, M.; Heberle, J.; Bittner, A. M.; Hillenbrand, R. Structural Analysis and Mapping of Individual Protein Complexes by Infrared Nanospectroscopy. *Nat. Commun.* **2013**, *4* (1), 2890.
(6) Amenabar, I.; Poly, S.; Goikoetxea, M.; Nuansing, W.; Lasch, P.; Hillenbrand, R. Hyperspectral Infrared Nanoimaging of Organic Samples Based on Fourier Transform Infrared Nanospectroscopy. *Nat. Commun.* **2017**, *8* (1), 14402.
(7) Fei, Z.; Rodin, A. S.; Andreev, G. O.; Bao, W.; McLeod, A. S.; Wagner, M.; Zhang, L. M.; Zhao, Z.; Thiemens, M.; Dominguez, G.; Fogler, M. M.; Neto, A. H. C.; Lau, C. N.; Keilmann, F.; Basov, D. N. Gate-Tuning of Graphene Plasmons Revealed by Infrared Nano-Imaging. *Nature* **2012**, *487* (7405), 82−85.
(8) Chen, J.; Badioli, M.; Alonso-González, P.; Thongrattanasiri, S.; Huth, F.; Osmond, J.; Spasenović, M.; Centeno, A.; Pesquera, A.; Godignon, P.; Zurutuza Elorza, A.; Camara, N.; de Abajo, F. J. G.; Hillenbrand, R.; Koppens, F. H. L. Optical Nano-Imaging of Gate-Tunable Graphene Plasmons. *Nature* **2012**, *487* (7405), 77−81.
(9) Dai, S.; Fei, Z.; Ma, Q.; Rodin, A. S.; Wagner, M.; McLeod, A. S.; Liu, M. K.; Gannett, W.; Regan, W.; Watanabe, K.; Taniguchi, T.; Thiemens, M.; Dominguez, G.; Neto, A. H. C.; Zettl, A.; Keilmann, F.; Jarillo-Herrero, P.; Fogler, M. M.; Basov, D. N. Tunable Phonon Polaritons in Atomically Thin van Der Waals Crystals of Boron Nitride. *Science* **2014**, *343* (6175), 1125−1129.
(10) Basov, D. N.; Fogler, M. M.; Garcia de Abajo, F. J. Polaritons in van Der Waals Materials. *Science* **2016**, *354* (6309), aag1992−aag1992.
(11) Huber, A. J.; Keilmann, F.; Wittborn, J.; Aizpurua, J.; Hillenbrand, R. Terahertz Near-Field Nanoscopy of Mobile Carriers in Single Semiconductor Nanodevices. *Nano Lett.* **2008**, *8* (11), 3766−3770.
(12) Stiegler, J. M.; Huber, A. J.; Diedenhofen, S. L.; Gómez Rivas, J.; Algra, R. E.; Bakkers, E. P. A. M.; Hillenbrand, R. Nanoscale Free-Carrier Profiling of Individual Semiconductor Nanowires by Infrared Near-Field Nanoscopy. *Nano Lett.* **2010**, *10* (4), 1387−1392.
(13) Ritchie, E. T.; Hill, D. J.; Mastin, T. M.; Deguzman, P. C.; Cahoon, J. F.; Atkin, J. M. Mapping Free-Carriers in Multijunction Silicon Nanowires Using Infrared Near-Field Optical Microscopy. *Nano Lett.* **2017**, *17* (11), 6591−6597.
(14) Qazilbash, M. M.; Brehm, M.; Chae, B.-G.; Ho, P.-C.; Andreev, G. O.; Kim, B.-J.; Yun, S. J.; Balatsky, A. V.; Maple, M. B.; Keilmann, F.; Kim, H.-T.; Basov, D. N. Mott Transition in VO2 Revealed by Infrared Spectroscopy and Nano-Imaging. *Science* **2007**, *318* (5857), 1750−1753.
(15) Jones, A. C.; Berweger, S.; Wei, J.; Cobden, D.; Raschke, M. B. Nano-Optical Investigations of the Metal−Insulator Phase Behavior of Individual VO_2 Microcrystals. *Nano Lett.* **2010**, *10* (5), 1574−1581.
(16) Liu, M.; Sternbach, A. J.; Basov, D. N. Nanoscale Electrodynamics of Strongly Correlated Quantum Materials. *Rep. Prog. Phys.* **2017**, *80* (1), 014501.
(17) Sterl, F.; Linnenbank, H.; Steinle, T.; Mörz, F.; Strohfeldt, N.; Giessen, H. Nanoscale Hydrogenography on Single Magnesium Nanoparticles. *Nano Lett.* **2018**, *18* (7), 4293−4302.
(18) Knoll, B.; Keilmann, F. Enhanced Dielectric Contrast in Scattering-Type Scanning near-Field Optical Microscopy. *Opt. Commun.* **2000**, *182* (4), 321−328.
(19) Hillenbrand, R.; Keilmann, F. Complex Optical Constants on a Subwavelength Scale. *Phys. Rev. Lett.* **2000**, *85* (14), 3029−3032.
(20) Keilmann, F.; Hillenbrand, R. Near-Field Microscopy by Elastic Light Scattering from a Tip. *Philos. Trans. R. Soc., A* **2004**, *362* (1817), 787−805.
(21) Pollard, B.; Muller, E. A.; Hinrichs, K.; Raschke, M. B. Vibrational Nano-Spectroscopic Imaging Correlating Structure with Intermolecular Coupling and Dynamics. *Nat. Commun.* **2014**, *5* (1), 3587.
(22) Huth, F.; Chuvilin, A.; Schnell, M.; Amenabar, I.; Krutokhvostov, R.; Lopatin, S.; Hillenbrand, R. Resonant Antenna Probes for Tip-Enhanced Infrared Near-Field Microscopy. *Nano Lett.* **2013**, *13* (3), 1065−1072.
(23) Jones, A. C.; Raschke, M. B. Thermal Infrared Near-Field Spectroscopy. *Nano Lett.* **2012**, *12* (3), 1475−1481.
(24) Huth, F.; Schnell, M.; Wittborn, J.; Ocelic, N.; Hillenbrand, R. Infrared-Spectroscopic Nanoimaging with a Thermal Source. *Nat. Mater.* **2011**, *10* (5), 352−356.
(25) Wagner, M.; Jakob, D. S.; Horne, S.; Mittel, H.; Osechinskiy, S.; Phillips, C.; Walker, G. C.; Su, C.; Xu, X. G. Ultrabroadband Nanospectroscopy with a Laser-Driven Plasma Source. *ACS Photonics* **2018**, *5* (4), 1467−1475.
(26) Lahneman, D. J.; Huffman, T. J.; Xu, P.; Wang, S. L.; Grogan, T.; Qazilbash, M. M. Broadband Near-Field Infrared Spectroscopy with a High Temperature Plasma Light Source. *Opt. Express* **2017**, *25* (17), 20421−20430.
(27) Amarie, S.; Ganz, T.; Keilmann, F. Mid-Infrared near-Field Spectroscopy. *Opt. Express* **2009**, *17* (24), 21794−21801.

(28) Amarie, S.; Keilmann, F. Broadband-Infrared Assessment of Phonon Resonance in Scattering-Type near-Field Microscopy. *Phys. Rev. B: Condens. Matter Mater. Phys.* **2011**, *83* (4), 045404.
(29) Xu, X. G.; Rang, M.; Craig, I. M.; Raschke, M. B. Pushing the Sample-Size Limit of Infrared Vibrational Nanospectroscopy: From Monolayer toward Single Molecule Sensitivity. *J. Phys. Chem. Lett.* **2012**, *3* (13), 1836−1841.
(30) Bensmann, S.; Gaußmann, F.; Lewin, M.; Wüppen, J.; Nyga, S.; Janzen, C.; Jungbluth, B.; Taubner, T. Near-Field Imaging and Spectroscopy of Locally Strained GaN Using an IR Broadband Laser. *Opt. Express* **2014**, *22* (19), 22369−22381.
(31) Bechtel, H. A.; Muller, E. A.; Olmon, R. L.; Martin, M. C.; Raschke, M. B. Ultrabroadband Infrared Nanospectroscopic Imaging. *Proc. Natl. Acad. Sci. U. S. A.* **2014**, *111* (20), 7191−7196.
(32) Hermann, P.; Hoehl, A.; Patoka, P.; Huth, F.; Rühl, E.; Ulm, G. Near-Field Imaging and Nano-Fourier-Transform Infrared Spectroscopy Using Broadband Synchrotron Radiation. *Opt. Express* **2013**, *21* (3), 2913−2919.
(33) Ikemoto, Y.; Ishikawa, M.; Nakashima, S.; Okamura, H.; Haruyama, Y.; Matsui, S.; Moriwaki, T.; Kinoshita, T. Development of Scattering Near-Field Optical Microspectroscopy Apparatus Using an Infrared Synchrotron Radiation Source. *Opt. Commun.* **2012**, *285* (8), 2212−2217.
(34) Hermann, P.; Hoehl, A.; Ulrich, G.; Fleischmann, C.; Hermelink, A.; Kästner, B.; Patoka, P.; Hornemann, A.; Beckhoff, B.; Rühl, E.; Ulm, G. Characterization of Semiconductor Materials Using Synchrotron Radiation-Based near-Field Infrared Microscopy and Nano-FTIR Spectroscopy. *Opt. Express* **2014**, *22* (15), 17948−17958.
(35) Govyadinov, A. A.; Amenabar, I.; Huth, F.; Carney, P. S.; Hillenbrand, R. Quantitative Measurement of Local Infrared Absorption and Dielectric Function with Tip-Enhanced Near-Field Microscopy. *J. Phys. Chem. Lett.* **2013**, *4* (9), 1526−1531.
(36) Lucas, I. T.; McLeod, A. S.; Syzdek, J. S.; Middlemiss, D. S.; Grey, C. P.; Basov, D. N.; Kostecki, R. IR Near-Field Spectroscopy and Imaging of Single $Li_x FePO_4$ Microcrystals. *Nano Lett.* **2015**, *15* (1), 1−7.
(37) Gamage, S.; Howard, M.; Makita, H.; Cross, B.; Hastings, G.; Luo, M.; Abate, Y. Probing Structural Changes in Single Enveloped Virus Particles Using Nano-Infrared Spectroscopic Imaging. *PLoS One* **2018**, *13* (6), e0199112.
(38) Szostak, R.; Silva, J. C.; Turren-Cruz, S.-H.; Soares, M. M.; Freitas, R. O.; Hagfeldt, A.; Tolentino, H. C. N.; Nogueira, A. F. Nanoscale Mapping of Chemical Composition in Organic-Inorganic Hybrid Perovskite Films. *Sci. Adv.* **2019**, *5* (10), eaaw6619.
(39) Ryu, M.; Honda, R.; Cernescu, A.; Vailionis, A.; Balčytis, A.; Vongsvivut, J.; Li, J.-L.; Linklater, D. P.; Ivanova, E. P.; Mizeikis, V.; Tobin, M. J.; Morikawa, J.; Juodkazis, S. Nanoscale Optical and Structural Characterisation of Silk. *Beilstein J. Nanotechnol.* **2019**, *10*, 922−929.
(40) Meyns, M.; Primpke, S.; Gerdts, G. Library Based Identification and Characterisation of Polymers with Nano-FTIR and IR-SSNOM Imaging. *Anal. Methods* **2019**, *11* (40), 5195−5202.
(41) Li, P.; Lewin, M.; Kretinin, A. V.; Caldwell, J. D.; Novoselov, K. S.; Taniguchi, T.; Watanabe, K.; Gaussmann, F.; Taubner, T. Hyperbolic Phonon-Polaritons in Boron Nitride for near-Field Optical Imaging and Focusing. *Nat. Commun.* **2015**, *6* (1), 7507.
(42) Shi, Z.; Bechtel, H. A.; Berweger, S.; Sun, Y.; Zeng, B.; Jin, C.; Chang, H.; Martin, M. C.; Raschke, M. B.; Wang, F. Amplitude- and Phase-Resolved Nanospectral Imaging of Phonon Polaritons in Hexagonal Boron Nitride. *ACS Photonics* **2015**, *2* (7), 790−796.
(43) Yoxall, E.; Schnell, M.; Nikitin, A. Y.; Txoperena, O.; Woessner, A.; Lundeberg, M. B.; Casanova, F.; Hueso, L. E.; Koppens, F. H. L.; Hillenbrand, R. Direct Observation of Ultraslow Hyperbolic Polariton Propagation with Negative Phase Velocity. *Nat. Photonics* **2015**, *9* (10), 674−678.
(44) Foteinopoulou, S.; Devarapu, G. C. R.; Subramania, G. S.; Krishna, S.; Wasserman, D. Phonon-Polaritonics: Enabling Powerful Capabilities for Infrared Photonics. *Nanophotonics* **2019**, *8* (12), 2129−2175.
(45) Basov, D. N.; Averitt, R. D.; van der Marel, D.; Dressel, M.; Haule, K. Electrodynamics of Correlated Electron Materials. *Rev. Mod. Phys.* **2011**, *83* (2), 471−541.
(46) Johnson, S. C.; Muller, E. A.; Khatib, O.; Bonnin, E. A.; Gagnon, A. C.; Raschke, M. B. Infrared Nanospectroscopic Imaging in the Rotating Frame. *Optica* **2019**, *6* (4), 424−429.
(47) Kästner, B.; Schmähling, F.; Hornemann, A.; Ulrich, G.; Hoehl, A.; Kruskopf, M.; Pierz, K.; Raschke, M. B.; Wübbeler, G.; Elster, C. Compressed Sensing FTIR Nano-Spectroscopy and Nano-Imaging. *Opt. Express* **2018**, *26* (14), 18115−18124.
(48) Schnell, M.; Carney, P. S.; Hillenbrand, R. Synthetic Optical Holography for Rapid Nanoimaging. *Nat. Commun.* **2014**, *5* (1), 3499.
(49) Deutsch, B.; Schnell, M.; Hillenbrand, R.; Carney, P. S. Synthetic Optical Holography with Nonlinear-Phase Reference. *Opt. Express* **2014**, *22* (22), 26621−26634.
(50) Schnell, M.; Perez-Roldan, M. J.; Carney, P. S.; Hillenbrand, R. Quantitative Confocal Phase Imaging by Synthetic Optical Holography. *Opt. Express* **2014**, *22* (12), 15267−15276.
(51) Canales-Benavides, A.; Zhuo, Y.; Amitrano, A. M.; Kim, M.; Hernandez-Aranda, R. I.; Carney, P. S.; Schnell, M. Accessible Quantitative Phase Imaging in Confocal Microscopy with Sinusoidal-Phase Synthetic Optical Holography. *Appl. Opt.* **2019**, *58* (5), A55−A64.
(52) Di Donato, A.; Farina, M. Synthetic Holography Based on Scanning Microcavity. *AIP Adv.* **2015**, *5* (11), 117125.
(53) Di Donato, A.; Tamagnone, M.; Criante, L.; Cavanini, L.; Mencarelli, D.; Ippoliti, G.; Pierantoni, L.; Orlando, G.; Morini, A.; Farina, M. Synthetic Optical Holography for In-Depth Imaging of Optical Vortices in Speckle Patterns. *AIP Adv.* **2019**, *9* (1), 015211.
(54) Mastel, S.; Govyadinov, A. A.; de Oliveira, T. V. A. G.; Amenabar, I.; Hillenbrand, R. Nanoscale-Resolved Chemical Identification of Thin Organic Films Using Infrared near-Field Spectroscopy and Standard Fourier Transform Infrared References. *Appl. Phys. Lett.* **2015**, *106* (2), 023113.
(55) Lyons, R. G. *Understanding Digital Signal Processing*, 3rd ed.; Prentice Hall: Upper Saddle River, NJ, 2011.
(56) Cahill, B. P. *Partially Coherent Fields in Synthetic Optical Holography*; University of Illinois: Urbana-Champaign, IL, 2016; http://hdl.handle.net/2142/92664.
(57) Hegenbarth, R.; Steinmann, A.; Mastel, S.; Amarie, S.; Huber, A. J.; Hillenbrand, R.; Sarkisov, S. Y.; Giessen, H. High-Power Femtosecond Mid-IR Sources for s-SNOM Applications. *J. Opt.* **2014**, *16* (9), 094003.

https://dx.doi.org/10.1021/acsphotonics.0c01164
ACS Photonics 2020, 7, 2878−2885